

Article

# Artificial Negative Polarity Thunderstorm Cell Modeling of Nearby Incomplete Upward Discharges' Influence on Elements of Monitoring Systems for Air Transmission Lines

Nikolay Lysov \*, Alexander Temnikov, Leonid Chernensky, Alexander Orlov, Olga Belova, Tatiana Kivshar, Dmitry Kovalev and Vadim Voevodin

Department of Electrophysics and High Voltage Technique, Moscow Power Engineering Institute, National Research University, 111250 Moscow, Russia; TemnikovAG@mpei.ru (A.T.); ChernenskyLL@mpei.ru (L.C.); OrlovAV@mpei.ru (A.O.); belovaos@mail.ru (O.B.); geratk@mail.ru (T.K.); kovalevdi@mpei.ru (D.K.); voevodinvv@mpei.ru (V.V.)

\* Correspondence: streamer.corona@gmail.com; Tel.: +7-9168456253

**Abstract:** The article represents results of a physical simulation of incomplete upward leader discharges induced on air transmission lines' elements, using charged artificial thunderstorm cells of negative polarity. The influence of such discharges on closely located model sensors (both of rod and elongated types) of digital monitoring systems, as well as on the models of receiver-transmission systems of local data collection (antennas), was determined. Effect of heterogeneity of electromagnetic field caused by incomplete upward discharges on frequency specter of signals generated on sensors and antennas was estimated. Wavelet analysis was carried out to determine the basic frequency diapasons of such signals. Based on experimental data obtained, suppositions about the extent of influence of nearby incomplete leader discharges on the functioning of currently used systems of transmission lines' monitoring were made.

**Keywords:** artificial thunderstorm cell; lightning; upward leader discharges; electromagnetic radiation spectrum; wavelet; transmission line monitoring system; model element; simulation



**Citation:** Lysov, N.; Temnikov, A.; Chernensky, L.; Orlov, A.; Belova, O.; Kivshar, T.; Kovalev, D.; Voevodin, V. Artificial Negative Polarity Thunderstorm Cell Modeling of Nearby Incomplete Upward Discharges' Influence on Elements of Monitoring Systems for Air Transmission Lines. *Energies* **2021**, *14*, 7100. <https://doi.org/10.3390/en14217100>

Academic Editor: Dan Doru Micu

Received: 31 August 2021

Accepted: 26 October 2021

Published: 31 October 2021

**Publisher's Note:** MDPI stays neutral with regard to jurisdictional claims in published maps and institutional affiliations.



**Copyright:** © 2021 by the authors. Licensee MDPI, Basel, Switzerland. This article is an open access article distributed under the terms and conditions of the Creative Commons Attribution (CC BY) license (<https://creativecommons.org/licenses/by/4.0/>).

## 1. Introduction

Remote monitoring systems are increasingly being introduced into the management of transmission lines and become an important element of digital power industry [1–11]. During their exploitation, it was observed that the functionality of the artificial intelligence elements used in such systems (i.e., all devices that contain electromagnetic parts, e.g., sensors; analog–digital converters for processing of recorded signals; antennas, etc.) may be compromised under the influence of lightning and atmospheric electricity [3,11,12]. It is not entirely clear how the discharge phenomena forming on both rod and elongated ground objects under the influence of thunderclouds and lightning (e.g., flashes of streamer corona, ascending leaders, the main discharge) and the electromagnetic radiation they create will affect functioning of such elements [13,14]. The purpose of this work is to estimate the influence of electromagnetic radiation emerged from incomplete upward leader discharge phenomena, located close to the remote monitoring system, on the system's elements. To achieve this goal, a thunderstorm experimental environment was modeled using artificially created thunderstorm cells of negative polarity. This work is a continuation of [15], where the characteristics of streamer discharges that did not pass into the ascending leader were considered.

## 2. Experimental Complex and Experiment Schemes

Physical processes were modeled on experimental measurement complex “Thunderstorm” [16], as in the scheme of Figure 1.

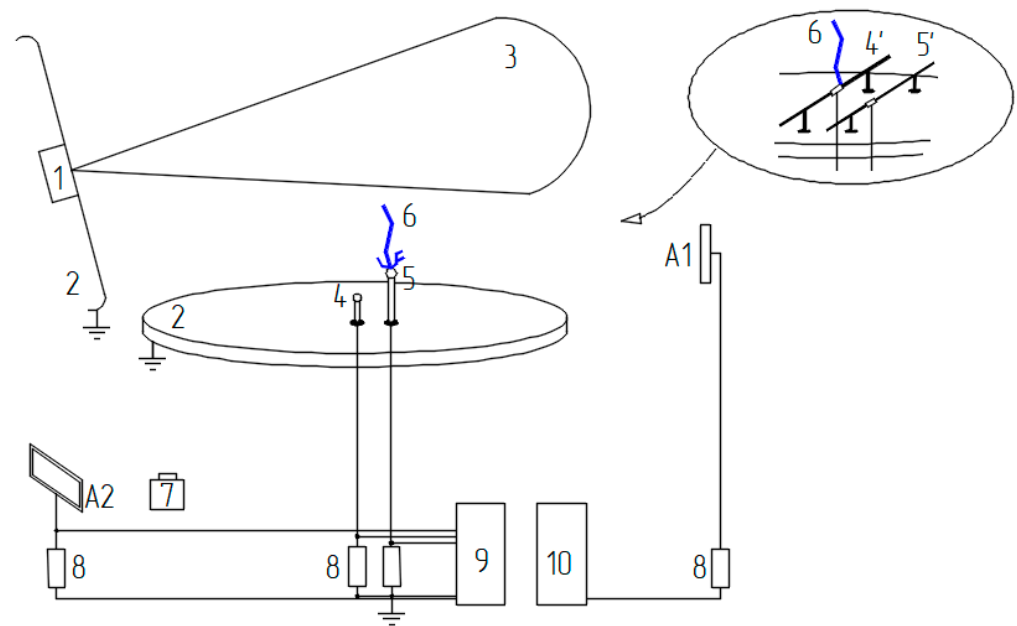


**Figure 1.** First scheme of experimental and measurement setup: 1—charged aerosol generator, 2—grounded electrostatic screens, 3—artificial thunderstorm cell, 4, 5—rod electrodes, 4', 5'—elongated electrodes, 6—upward discharge phenomena, 7—digital camera Panasonic DMC-50, 8—shunts, 9, 10—digital memory oscilloscopes Tektronix TDS 3054B и Tektronix DPO 7254, A1, A2—flat antennas.

Experimental measurement complex “Thunderstorm” was created at the Department of Electrophysics and High Voltage Technique (National Research University “Moscow Power Engineering Institute”) with the purpose of physical modeling and exploration of fundamental and practical problems in the fields of atmospheric electricity, lightning physics, and lightning protection of both grounded and flying objects [17–21]. It allows creating artificial clouds from a highly charged water aerosol with the maximal density of the volume charge (the artificial thunderstorm cells), which are equal to the electrically charged thunderclouds. Due to the capacity to create artificial thunderstorm cells of both polarities, located above each other, the complex allows to generate different types of electric discharges characteristic of thunderclouds, from weak diffuse discharges to the main stage of discharge with high current release.

Experimental investigational complex “Thunderstorm” consists of an aerosol camera (volume  $> 120 \text{ m}^3$ ), generator of charged aerosol, investigational object (the studied system of electrodes), and measuring complex. In the aerosol camera, two varieties of artificial aerosol clouds (artificial thunderstorm cells) were used: either a one-cell structure of negative or positive polarity, or two-cell structure consisting of two artificial thunderstorm cells of the same or different polarities, located above ground at different heights [22,23].

A condensational generator of charged water aerosol was used to create artificial thunderstorm cells. When the pressure in the generator was between 4 and 10 bar, the velocity of water steam efflux from subsonic convergent nozzle was around 400 m/s. Water aerosol particles were charged by condensation on ions and ion charge in the field of corona discharge occurring in the nozzle exit section.

The charged aerosol generator maintained an outlet current in a broad diapason from  $10 \mu\text{A}$  to  $150 \mu\text{A}$ . As a result of variations in the generator’s outlet current, the charge of an individual artificial thunder cell could be regulated in a broad value diapason, reaching up to several hundreds of microcoulombs (at maximal charging currents). Volume density of charge in the central area of the cloud was in the diapason of  $1.5 \times 10^{-4}$ – $1.5 \times 10^{-2} \text{ C/m}^3$ . Each of the charged aerosol clouds is several cubic meters in volume. The lower cell is

located approximately at the 1 m height over the grounded plane, while the higher cell is located at the 2.1 m height.

When the generator is working at a high outlet current, the maximum potential of a single artificial thunderstorm cell may reach up to 1.0–1.5 MB [24–27]. As a result, a strong electric field is formed in the area between the artificial thunderstorm cell and the grounded plane. Its intensity reaches up to 6–10 kV/cm close to the ground and up to 17–20 kV/cm at the cell's lower border. Moreover, the electric field of the almost quasi-homogeneous quality is formed in the area between the cell's lower border and the ground plane at the height up to 0.4 cm from the ground, and at a distance of 1.0 to 2.0 m from the generator's nozzle [24,27]. The value of electric field's intensity in this area changes comparatively slowly as the height grows (30–40% increase). Due to this, investigative objects located in this area (e.g., rod or other electrodes up to 0.4 m in height) will be similarly affected by the electric field of the charged aerosol cloud.

The dynamics of electric field formation in the area between the artificial thunderstorm cell and the ground shows that 50 ms after the beginning of the water aerosol flow charging, field intensity at the ground under the charging cell increases to 1 kV/cm, and one second after, it may be more than 5–6 kV/cm [25–27]. By this time, the electric field intensity at the lower border of the artificial thunderstorm cell's charged areas is 10–12 kV/cm. These conditions facilitate discharge formation on the model investigative objects located on the grounded plane.

Therefore, a slow increase in the electric field's intensity is observed in the significant area of the space between an artificial thunderstorm cell and ground. Due to the inertial character of the charged cloud formation and existence of negative feedback between the cell and occurring discharge phenomena, it can thus be expected that all discharge processes in the space between the cell and grounded model object will occur and develop under minimal required conditions practically without overvoltage. In this case, the character of distribution and value of electric field's intensity between an artificial thunderstorm cell and the grounded plane are comparable to characteristics of the field under a real thundercloud. Such a field is characteristic of the conditions when a thundercloud (or a downward lightning leader beginning to develop from the cloud) affects all above-ground objects [28]. By changing the generator's outlet current, it is possible to emulate the development of all types of sparks characteristic for a thunderstorm, including leader stage and main discharge.

Figures 2–4 demonstrate photos of the different discharge phenomena, forming either between cells of different polarity or between cells and grounded objects. In recent years, a similar complex based on a generator of charged aerosol has been used in Istra (Moscow region) (Rakov V.A., Syssoev V.S., Kostinskiy A.Y. et al. [29–34]). This generator was also developed at the Department of Electrophysics and High Voltage Technique (National Research University "Moscow Power Engineering Institute").

More than 90% of the lightning strikes into the ground are negative. This is related to the characteristic thundercloud structure, where, in the majority of cases, the main negative charge is located in its lower half [28,35]. Its impact leads not only to initiation and formation of the downward lightning leader, but also to initiation and formation of the upward discharges, including incomplete and/or counterpart positive streamer and leader discharges in the opposite direction from the structural elements of objects located on the ground under the thundercloud [35]. This is why an artificial thunder cell of negative polarity was used for the physical modelling of the possible effect of incomplete upward streamer and leader discharges on the nearby located various elements of power lines' monitoring systems. At the same time, the artificial thunderstorm cell charge (outlet current of aerosol generator) was maintained at a level where the probability of upward discharges' transition into a high-powered main stage was minimal.

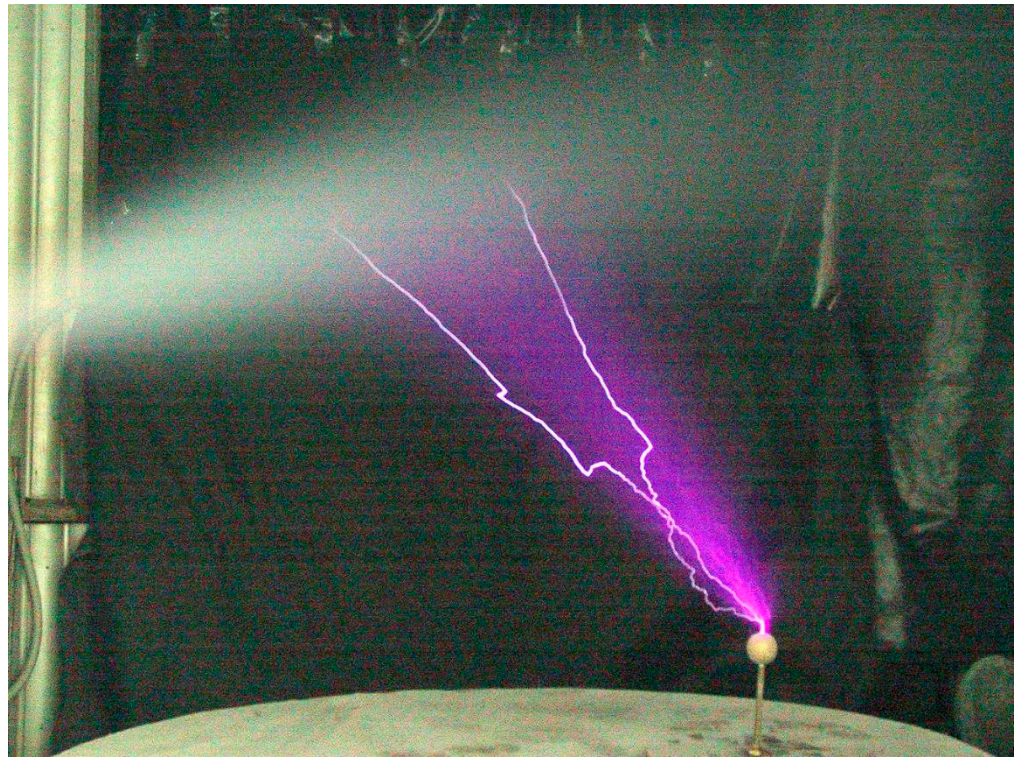


**Figure 2.** Characteristic picture of the discharge formation between artificial thunderstorm cell of negative polarity and the ground.



**Figure 3.** Characteristic picture of the discharge formation between positively and negatively charged artificial thunderstorm cells, using model hydrometeor groups.



**Figure 4.** Characteristic picture of the discharge formation between the system of artificial thunderstorm cells of negative polarity and the ground.

The potential of the artificial thunderstorm cell of negative polarity reached up to 1.2 MV. Monitoring system elements and grounded parts of air transmission lines were modeled using rod electrodes with spherical tops or appeared as a cylindrical element isolated from the main part of the whole construction (Figure 1). When discharge phenomena appeared at one of the electrodes, its parameters were registered, as well as the aimed signals at the nearest electrode.

Two experimental series were conducted while modeling the effect of close incomplete upward discharges on the elements of power lines' monitoring systems using artificial thunderstorm cells. In the first series, an experimental scheme with two rod model electrodes with different amplification coefficients (AQ) was used. This series has modeled signals induced on rod sensor models (receiver–transmitter devices) by the electromagnetic radiation of the upward leader discharges forming from the nearby rod elements. In the second series, a similar experimental scheme was used, substituting rod elements with elongated (cylindric) models.

Tops of rod electrodes were electrically isolated from their bodies in order to decrease the influence of the electric induction current on the electrical characteristics of the upward leader discharges forming from the top of the grounded model object, or to extract the signals induced by the nearby upward leader discharge specifically on the rod model sensor. The middle part of the elongated model conductors was isolated from the other parts with the same purpose.

Radius of the spheric (or conic, in case of small radii of curve slope) top of model rod electrodes varied in diapason from 0.3 cm to 2.5 cm. Rod electrode height varied from 16 cm to 40 cm. Radii of metal tubes modelling cylindric sensor elements, phase wires, and ground wires varied from 0.5 cm to 2.5 cm. Elongated electrodes were located at the height between 15 and 37 cm. AQ for model electrodes was calculated according to specialized software BETAFields.

Electrical characteristics of discharge phenomena between artificial thunderstorm cell and grounded model electrodes were registered based on measuring the following parameters:

- (1) Discharge current initiated at the ground model elements,

- (2) Electric induction current inflicted by discharge phenomena on the nearest models of digital objects and systems (sensors and antennas).

Both types of currents were measured using special low-inductance shunts.

During the experiment, the radii of the vertices of rod model objects and the radii of model cylindrical objects varied. This was done in order to model the situation when, under the influence of atmospheric electricity, discharge phenomena form on the digital elements and systems, which have substantially different electric field AQs. During statistical analysis the difference between the objects was taken into account by dividing them into groups according to this coefficient: group I— $AQ < 12$ ; group II— $12 < AQ < 27$ ; and group III— $AQ > 27$ .

The following variants of discharge phenomena formation next to digital objects were modeled in this work:

- Streamer corona and upward leader discharge form under the influence of a thundercloud's electromagnetic field on a grounded object (e.g., transmission tower). Electromagnetic radiation from the upward discharge affects the functioning of the sensors and antennas located on or close to the tower (Figure 5a),
- Streamer corona and upward leader discharge form under the influence of a thundercloud's electromagnetic field on a middle segment of a lightning protection wire. This affects the functioning of the sensors and antennas located in the middle segment of the phase wire (Figure 5b).

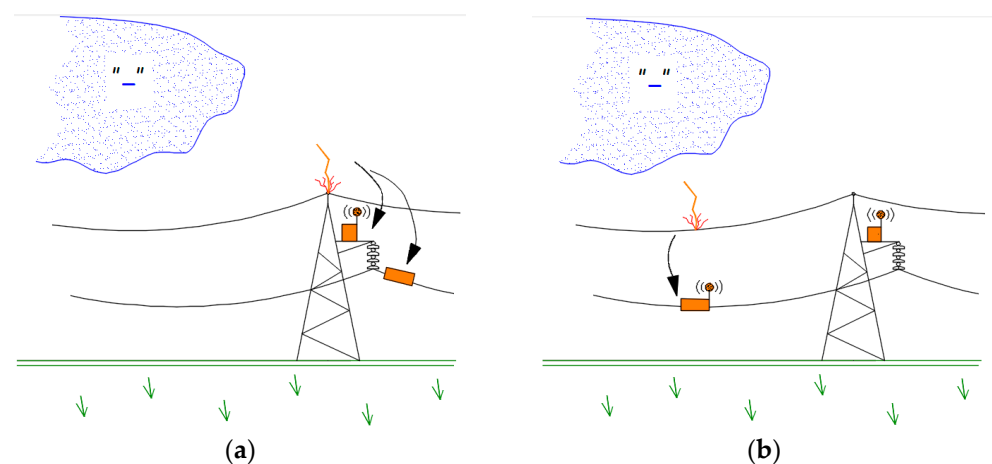


**Figure 5.** Variants of formation of discharge phenomena affecting power lines' digital monitoring systems: (a) streamer corona/upward leader discharge forms on a transmission tower, (b) streamer corona/upward leader discharge forms on a middle segment of a lightning protection wire.

Figures 6 and 7 represent photos of discharge phenomena that developed on the rod and elongated model electrodes while using the "Thunderstorm" experimental complex. It is clear that the discharge develops only on one of the two model electrodes. Photos were taken on a digital camera in long-exposure mode, which was set to turn on at the same time as the artificial thunderstorm cell's charging process began. This allowed documenting all development stages of the discharge phenomena generated on every element in the experimental area.

Figure 8 represents a characteristic oscillograph chart for the current of streamer flash and incomplete upward leader discharge and signals induced on the nearby grounded element and antennas. The following parameters were registered for the current signal: current amplitude, maximal velocity of current build-up, impulse charge, and total impulse length.

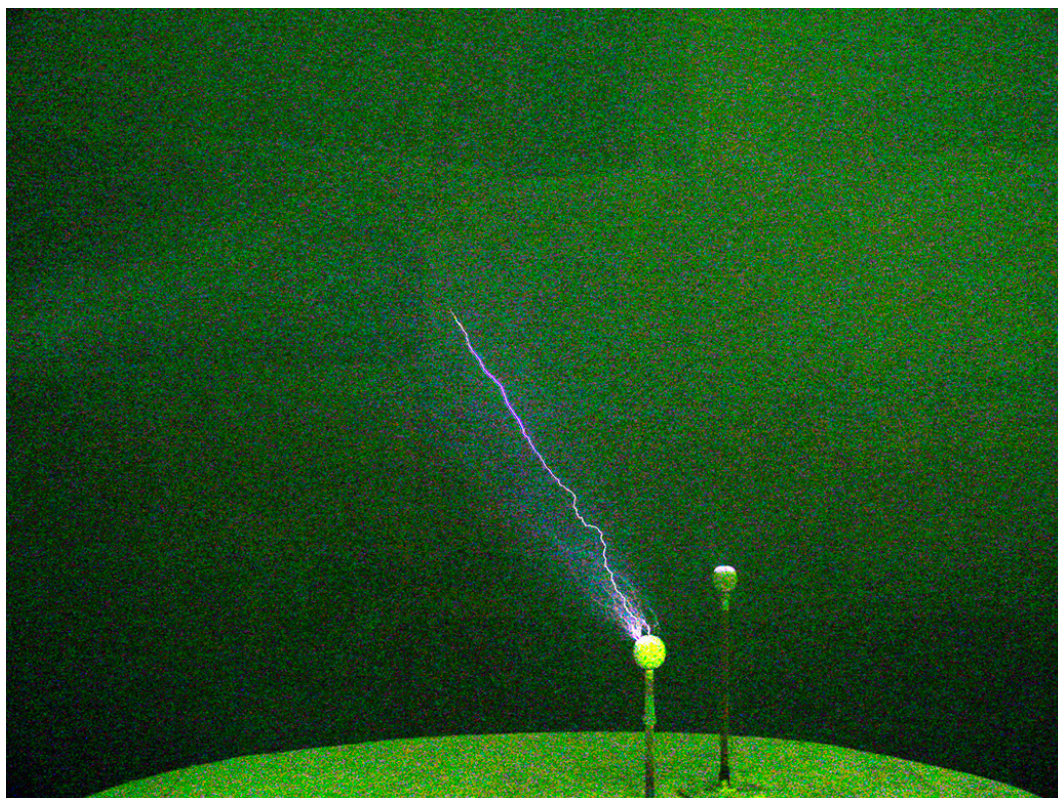


**Figure 6.** Upward leader discharges from the grounded rod model elements.

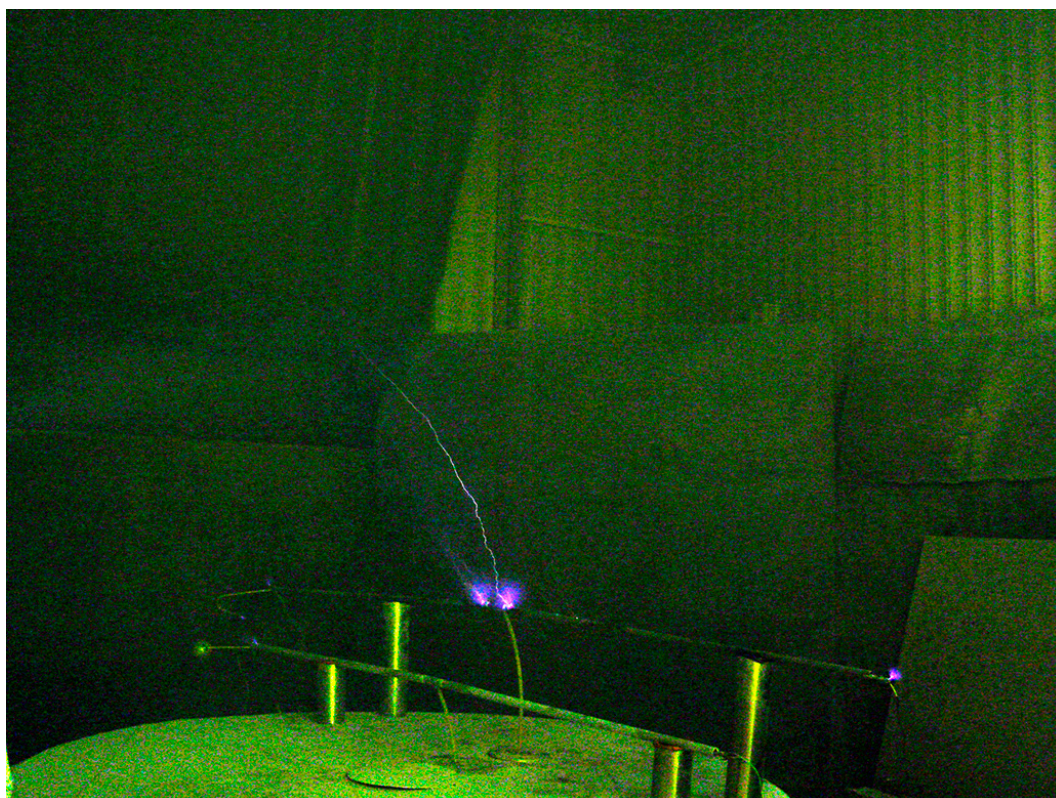


**Figure 7.** Upward leader discharges from the grounded cylinder model element.

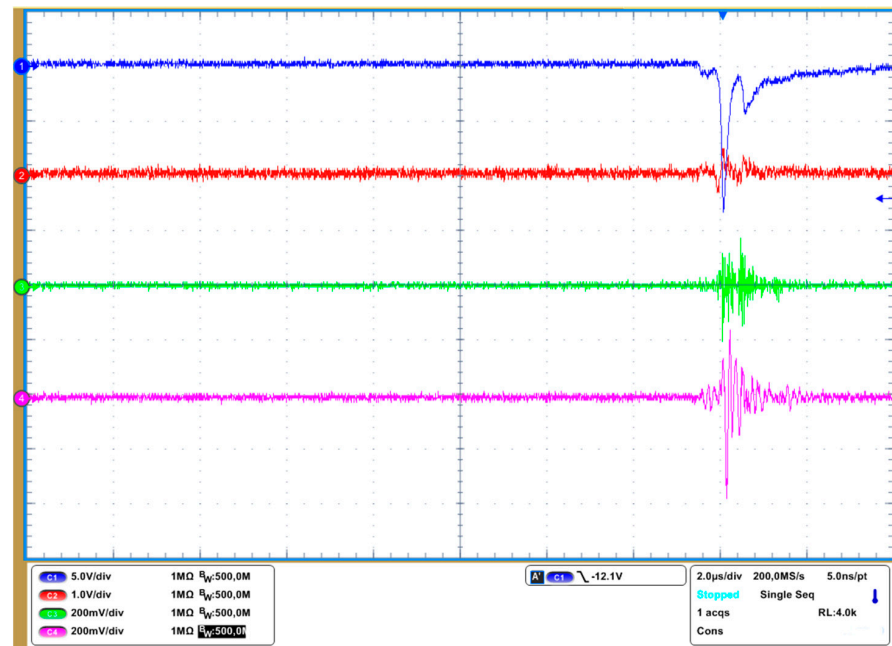


**Figure 8.** Characteristic oscillograph charts for discharge current from grounded electrode (channel 1), and electric induction currents induced on nearby electrode (channel 2) and flat antennas (channels 3 and 4).

Spectral characteristics of the induced signal were determined using software created specifically for this purpose. It was based on the Mexican hat wavelet analysis [36–38]. Upper level of the characteristic frequency, maximal intensity, and frequency of the maximal intensity in the wavelet spectrum have been determined. Characteristic wavelet spectrums for the currents and induced signal presented in Figure 9 are shown in Figures 10 and 11, correspondingly. These signals correlate to the signals from channels 1 and 2, represented in Figure 8.

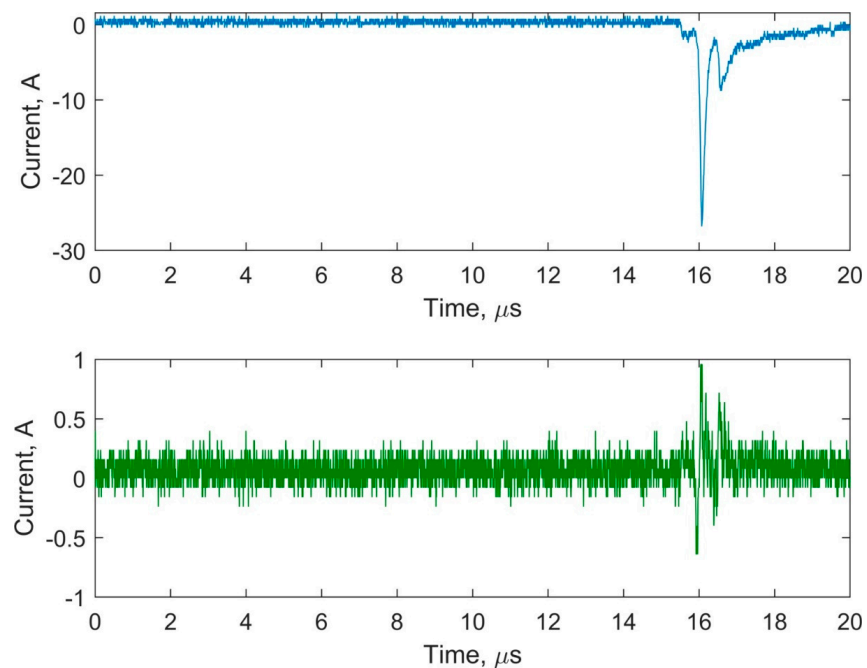


**Figure 9.** Oscillograms of the upward discharge current (**upper**) and induced electromagnetic effects (**bottom**).

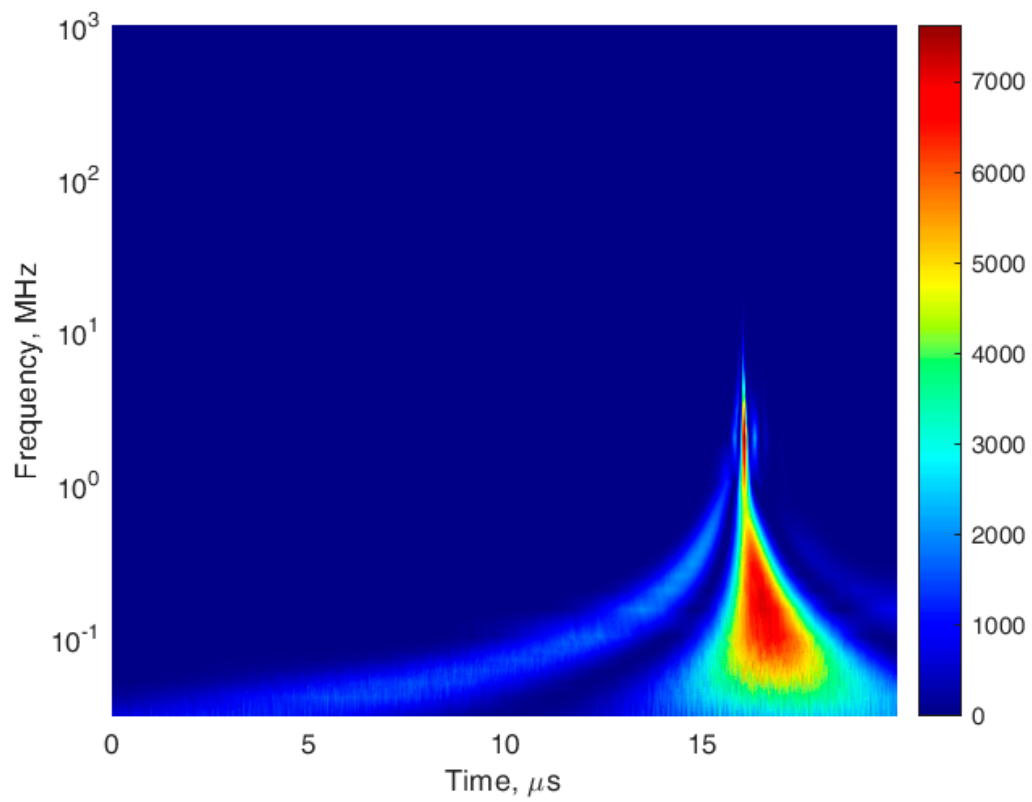


Figure 10. Wavelet spectrum of upward discharge current.

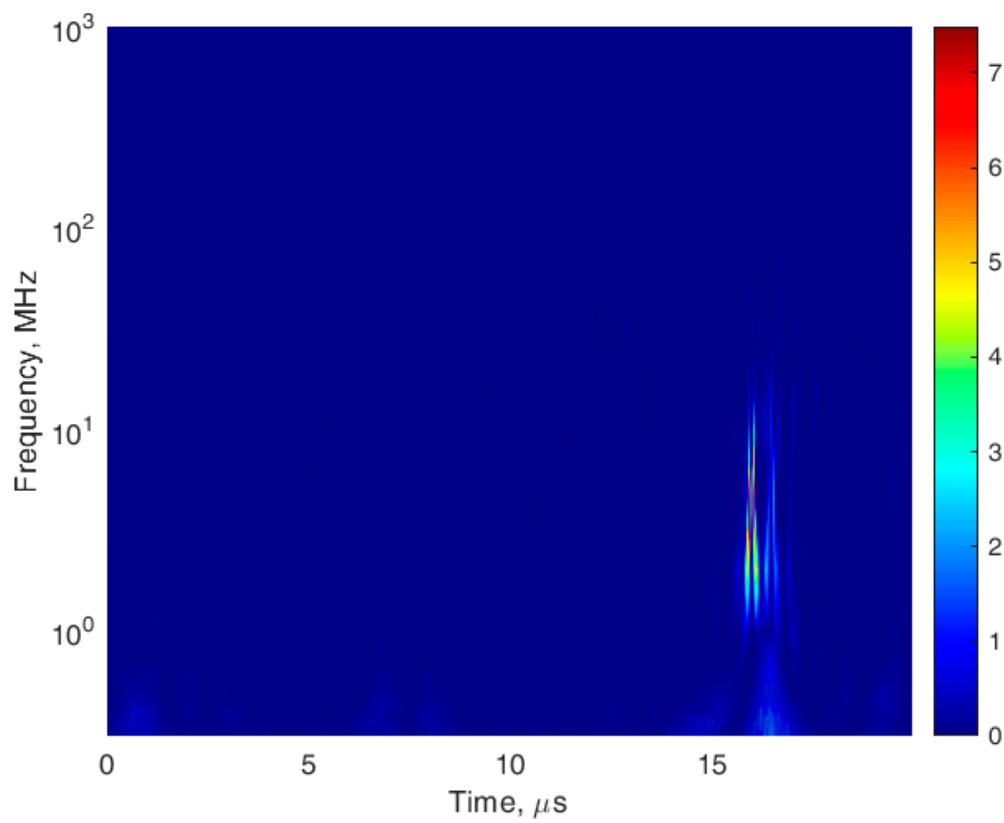


Figure 11. Wavelet spectrum of the signal induced on the nearby model element by the upward discharge.

### 3. Results

More than 300 experiments were completed and analyzed for this work. The parameters of electrode systems and their location in relation to each other varied through the experiments. Tables 1 and 2 represent results of processed signals and their wavelet analysis.

**Table 1.** Parameters of signals induced on model rod and elongated elements by a closely located flash of upward discharge (average values).

Source of Effect	Upward Discharge (Rod)		Upward Discharge (Elongated)		
	Amplification Coefficient	$\Delta T, \mu s$	$ I_{max} , A$	$\Delta T, \mu s$	$ I_{max} , A$
Group I		1.2	0.9	1.1	1.2
Group II		0.3	1.6	0.5	1.3
Group III		0.7	1.0	1.0	1.2

**Table 2.** Parameters of signals induced on flat antennas with upward discharge (average values).

Antenna	A1		A2	
Parameters	$\Delta T, ms$	$ I_{max} , A$	$\Delta T, \mu s$	$ I_{max} , A$
Average	1.1	1.1	1.8	1.8
Maximum	4.5	3.1	9.8	3.3

Analysis of spectral parameters of the signals induced on rod and elongated model elements, as incomplete upward discharges form on the nearby located model electrodes, has shown that the surrounding electrical field is considerably influenced by those discharges. Table 3 shows analysis results divided into three groups, depending on the value of electric field's amplification coefficient (AQ).

**Table 3.** Spectral parameters of signals induced with upward discharge (average values).

Source of Effect	Rod Elements			Elongated Elements			Antennas		
	AQ	Group I	Group II	Group III	Group I	Group II	Group III	A1	A2
$f_{max}, MHz$		122	756	391	119	785	467	602.3	144.4
$f(C_{max}), MHz$		11.1	77	14.7	9.6	73	12.3	51.6	10.5

During the experiments, several variants of elements' location in relation to each other were modeled. Receiver–transmitter devices (or other sensors) were located either very close to the place of discharge formation or at a longer distance from it (antenna A2). Another location variant had antennas located higher than the place of discharge formation (antenna A1 was located across from the lower cloud border of the artificial thunderstorm cell). This emulates, for example, natural conditions of a hilly or mountain scenery, high-rise objects, or the use of flying machines.

It is clear from the presented results that all variants of model rod and elongated elements of an intelligent monitoring system will be affected by nearby forming discharges, and that the induced signals will include frequency diapasons in hundreds of MHz up to GHz (Figure 12). When a flash of impulse streamer corona forms nearby, the values of maximal frequencies in the wavelet specter will be observed for model sensors with "average" amplification coefficients (group 2,  $12 < AQ < 27$ ): 756 MHz for rod elements and 785 MHz for elongated elements, on average. At the same time, on the model sensors with relatively low AQ (group 1,  $AQ < 12$ ) in most cases, maximal frequencies in the wavelet specter will not surpass 100 MHz (Figure 12). Unlike the cases when the streamer flash did not pass into the ascending leader [15], there are no frequencies more than

1 GHz in the specter of signals induced by the upward discharge (streamer flash plus the upward leader).

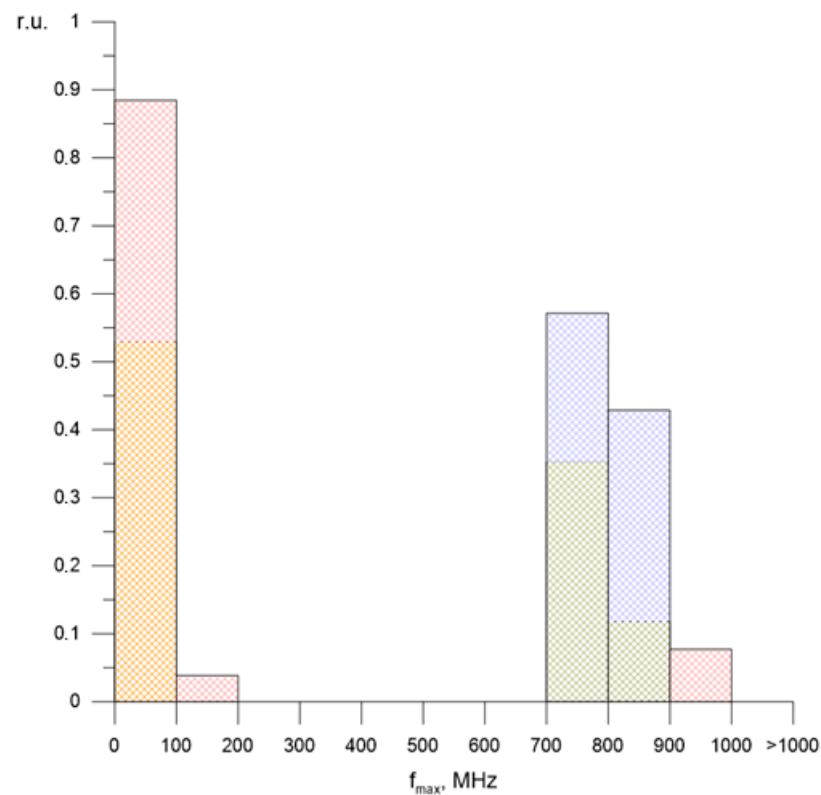


**Figure 12.** Histogram of diapasons of characteristic maximal frequencies in wavelet specter of the signals induced by close upward discharges on model elements of the rod and elongated types. Group 1—red; Group 2—blue; Group 3—yellow.

AN analogous tendency was discovered for the frequency corresponding to the maximum intensity of  $C_{max}$  ( $f(C_{max})$ ) in the wavelet specter (Figure 13): for the model elements in group 2, it was 77 MHz for rod elements and 73 MHz for elongated ones.

Wavelet specter analysis of signal, induced by closely located discharges on flat antennas, which model receiver–transmitter devices and other digital elements, has shown that frequencies of hundreds of MHz up to GHz are present in their specters, even during the primary part of upward discharge formation. Moreover, in the wavelet specter of signals induced on antennas by a close discharge formation, the frequencies  $f(C_{max})$  in the wavelet specter will average tens of MHz (Figures 14 and 15).

For avalanches that form and develop on electrodes of various sizes in electrical fields, their electromagnetic radiation (according to [39–44]) may be explicitly expressed in the diapasons from 4.0–5.0 MHz to 0.9–1.0 GHz. Characteristic frequency diapasons of wavelet specter signals (induced on model rod and elongated elements by the nearby discharges) correlate with this mechanism of electromagnetic radiation formation.

As shown by modelling [40–42], the specter of electromagnetic radiation of critical avalanche (which allows for its transition into a streamer) depends on the value of electric field intensity and on the particularities of the change in such field in the area where avalanches are formed. Probably, this is the reason for the very high frequencies detected in the wavelet specter of the signal induced on the model electrode by electromagnetic radiation of the nearby avalanche–streamer system of the upward discharge (impulse streamer corona plus the upward leader), forming on the electrodes with high AQ values (groups 2 and 3). Upward discharges forming on model elements with lower AQs (group 1), in the vicinity of which variation of field intensity occurs less rapidly, will induce the signals with lower frequency diapasons in their specters.

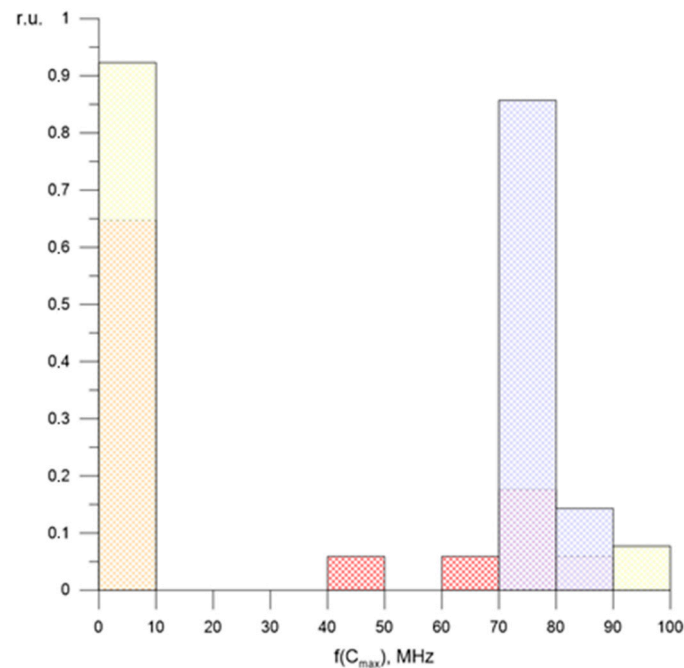


**Figure 13.** Histogram of  $f(C_{max})$  (frequency diapason corresponding to the maximum intensity of  $C_{max}$ ) in the wavelet specter of signals induced by the nearby located upward discharges on model elements of the rod and elongated types. Group 1—red; Group 2—blue; Group 3—yellow.

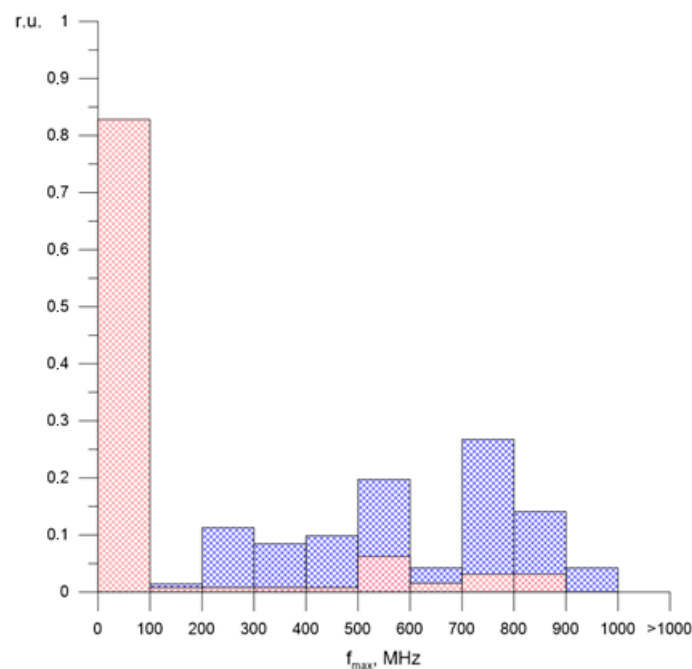


**Figure 14.** Histogram of diapasons of characteristic maximum frequencies in wavelet specter of signals induced on the flat antennas by a nearby discharge: antenna A1 (in blue); antenna A2 (in red).

It is also important to consider that, since the streamers form and develop by avalanches induced from their heads in electric fields of various size, electromagnetic radiation of those avalanches (according to [39–44]) may be explicitly expressed in diapasons from 0.5–1.0 MHz to 8–10 MHz.

During the formation of a specter of electromagnetic influence of the upward discharge developing between artificial thunderstorm cells and ground, the specter's ultrahigh frequency can also be affected by the powerful streamers of the upward leader reaching

to the cell borders. External electric field intensity next to these streamers rose up to 18–22 kV/cm. In such event, several avalanche-streamer strings will be located in this area at the same time. As noted in [39–44], in this case avalanches are situated close in time with each other, and their electromagnetic radiation fields almost overlap, which should lead to an increase in spectral amplitude.

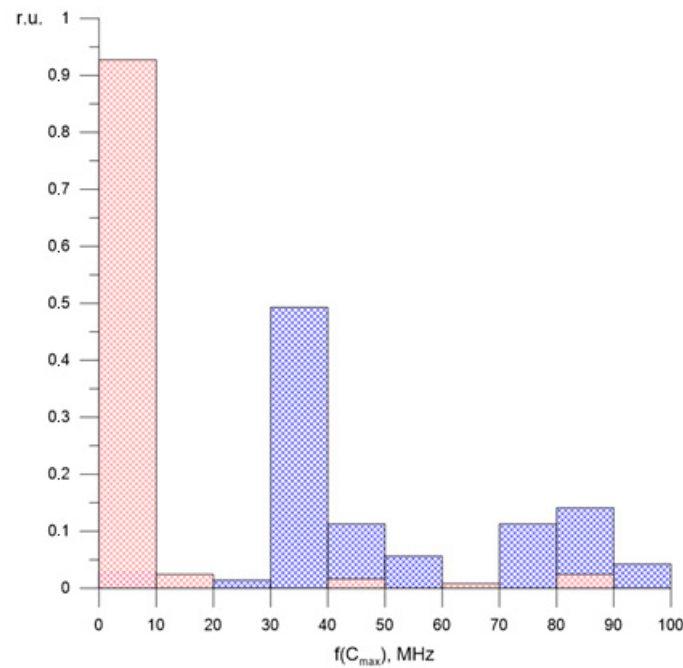


**Figure 15.** Histogram of diapasons of  $f(C_{max})$  in wavelet specter of signals induced on the flat antennas by a nearby discharge: antenna A1 (in blue); antenna A2 (in red).

#### 4. Discussion

Analysis of experimental data has shown the following characteristic spectral diapasons of signals induced on model rod objects of different AQ groups by the nearby streamer corona:

Group 1 objects:

Maximum frequencies ( $f_{max}$ ) in the wavelet specter of induced signals: 11–170 MHz; 900–1000 MHz. Frequencies corresponding to the maximal intensity of the wavelet specter ( $f(C_{max})$ ) of induced signals: 0.1–8 MHz; 90–100 MHz.

Group 2 objects:

$f_{max}$ : 765–833 MHz.  $f(C_{max})$ : 73–88 MHz.

Group 3 objects:

$f_{max}$ : 13–95 MHz; 717–845 MHz.  $f(C_{max})$ : 0.9–7 MHz; 40–50 MHz, 63–88 MHz.

Analysis of experimental data for model elongated elements (objects) of different AQ groups has shown:

Group 1 objects:

$f_{max}$ : 5–70 MHz; 900–1000 MHz.  $f(C_{max})$ : 0.7–9 MHz; 90–100 MHz.

Group 2 objects:

$f_{max}$ : 711–805 MHz.  $f(C_{max})$ : 70–82 MHz.

Group 3 objects:

$f_{max}$ : 4–75 MHz; 735–880 MHz.  $f(C_{max})$ : 0.3–6 MHz; 40–50 MHz.

In presence of the electromagnetic field generated by a thundercloud and lightning, incomplete upward discharges may form on different grounded objects. Electromagnetic radiation of such discharges, when they develop close to sensors of digital objects and systems, can create risks for the energetic safety of this equipment. The frequencies present

in the specter of the signal induced by the nearby streamer flash and upward leader on the sensors may affect their functioning and lead to errors in the collected data.

Such a problem is relevant for the sensors with frequency diapason under 100 kHz and under 1.5 GHz, which control isolation status of high voltage equipment and electromagnetic levels on substation switchyards. Such frequencies are typical for model elements (sensors) of all amplification coefficient groups [13,14]. Analogous errors may occur when electromagnetic radiation from the streamer corona flash and upward leader affects the type of system sensors which employs analog–digital converters (ADC) with working frequencies from several hundred kHz to several GHz in order to measure and further digitally process their signals [12,14]. Additionally, the aforementioned specters of signals induced by the streamer corona flashes transformed into upward leaders on rod sensors of monitoring, diagnostics, and management systems and may cause false reactions and errors for the systems that employ ADCs with working frequencies from several tens/hundreds Hz in slow high-voltage ADCs to several hundred MHz in high-velocity high-performance ADCs [12].

Electromagnetic radiation of incomplete upward discharges may lead to errors in monitoring systems using elongated sensors working in frequency diapasons under 1000 MHz (this relates to sensors belonging to all AQ groups) [3,13,14]. Using analog–digital converters with working frequencies from several hundred kHz to 1 GHz to process data from the signals may also lead to failures [12,14]. Additionally, aforementioned specters of signals induced by the streamer corona and upward leader discharges on elongated and rod sensors of monitoring systems may cause false reactions and errors for the systems that employ ADCs with working frequencies from several tens/hundreds Hz in slow high-voltage ADCs to several hundred MHz in high-velocity, high-performance ADCs [12].

Analysis of experimental data has shown the following characteristic spectral diapasons of signals induced on model flat broadband antennas by the nearby upward discharges:

Antenna A1:

f<sub>max</sub>: 111–955 MHz.

f(C<sub>max</sub>): 0.3–6 MHz; 28–60 MHz; 73–98 MHz.

Antenna A2:

f<sub>max</sub>: 21–852 MHz.

f(C<sub>max</sub>): 5–15 MHz; 48–88 MHz.

The electromagnetic radiation of incomplete upward discharges described above may also substantively affect receiver–transmitter devices (antennas) of digital systems and objects, which, in turn, may create risks for their energetic safety. Frequencies present in the specter of the signal induced on antennas by a nearby streamer flash and upward leader may lead to errors in their functioning, as well as distortion or loss of transmitted information [1,12]. Firstly, it may affect the data transmission channels using GSM (900/1100 MHz), as well as other systems of data transmission/reception working in MHz diapason. These may include:

- Transmission systems working from sensors with frequency of 915 MHz, located on air transmission lines [1];
- Systems, transmitting data on relatively small distances, e.g., using frequencies 434 MHz, 868 MHz for autonomous monitoring systems;
- Satellite connection systems, e.g., using user-accessible frequency diapason: Orbcomm system with frequencies of transmitters 137.0–138.0 MHz, 400.05–400.15 MHz, frequencies of terminals 148.0–150.05 MHz; “Gonets” system services its users in the diapasons of 0.2–0.3 GHz and 0.3–0.4 GHz [45,46].

## 5. Conclusions

Completed analysis of experimental data has allowed identifying the influence of close incomplete upward discharges (streamer flash plus the upward leader) on systems of monitoring, diagnostics, and management of the power objects. The influence of electromagnetic radiation of such discharges induced on the digital systems’ model sensors and

antennas (of both rod and elongated types) has been estimated. Characteristic diapasons of working frequencies of receiver–transmitter systems and digital–analog converters, where such influence is most substantial and may increase risks of failures and errors in their functioning, have been determined.

**Author Contributions:** Project administration, methodology A.T.; software, L.C. and O.B.; visualization, T.K.; investigation, A.O. and N.L.; writing—original draft preparation, V.V.; funding acquisition, D.K. All authors have read and agreed to the published version of the manuscript.

**Funding:** This study conducted by Moscow Power Engineering Institute was financially supported by the Ministry of Science and Higher Education of the Russian Federation (project No. FSWF-2020-0019).

**Institutional Review Board Statement:** Not applicable.

**Informed Consent Statement:** Not applicable.

**Data Availability Statement:** Not applicable.

**Conflicts of Interest:** The authors declare no conflict of interest.

## References

1. McCall, J.C.; Spillane, P.; Lindsey, K. Determining Crossing Conductor Clearance Using Line-Mounted LiDAR. In Proceedings of the CIGRE US National Committee 2015 Grid of the Future Symposium, Paris, France, 11–13 October 2015. Lindsey Publication Number 11T-001 CROSSING CONDUCTOR TLM.
2. Liu, Y.; Yin, H.; Wu, T. Transmission Line on-line Monitoring System Based on Ethernet and McWiLL. In Proceedings of the International Conference on Logistics Engineering, Management and Computer Science, Shenyang, China, 29–31 July 2015; pp. 680–683.
3. Working Group on Monitoring & Rating of Subcommittee 15.11 on Overhead Lines. Real-Time Overhead Transmission-Line Monitoring for Dynamic Rating. *IEEE Trans. Power Deliv.* **2016**, *31*, 921–927. [\[CrossRef\]](#)
4. Zhirui, L.; Shengsu, N.; Nan, J. Current Status and Development Trend of AC Transmission Line Parameter Measurement. *Autom. Electr. Power Syst.* **2017**, *41*, 181–191.
5. Hu, Y.; Liu, K. *Inspection and Monitoring Technologies of Transmission Lines with Remote Sensing*; Academic Press: Cambridge, MA, USA, 2017.
6. Li, S.; Li, J. Condition monitoring and diagnosis of power equipment: Review and prospective. *High Volt.* **2017**, *2*, 82–91. [\[CrossRef\]](#)
7. Singh, R.; Choudhury, S.; Gehlot, A. *Intelligent Communication, Control and Devices: Proceedings of the ICICCD 2017*; Springer Nature Singapore Pte Ltd.: Singapore, 2018.
8. Deng, C.-J. Challenges and Prospects of Power Transmission Line Intelligent Monitoring Technology. *Am. Res. J. Comput. Sci. Inf. Technol.* **2019**, *4*, 1–11.
9. Wydra, M.; Kubaczynski, P.; Mazur, K.; Ksiezopolski, B. Time-Aware Monitoring of Overhead Transmission Line Sag and Temperature with LoRa Communication. *Energies* **2019**, *12*, 505. [\[CrossRef\]](#)
10. Xing, Z.; Cui, W.; Liu, R.; Zheng, Z. Design and Application of Transmission Line Intelligent Monitoring System. *E3S Web Conf.* **2020**, *185*, 01063. [\[CrossRef\]](#)
11. Chen, H.; Qian, Z.; Liu, C.; Wu, J.; Li, W.; He, X. Time-Multiplexed Self-Powered Wireless Current Sensor for Power Transmission Lines. *Energies* **2021**, *14*, 1561. [\[CrossRef\]](#)
12. Ahmad, M.R.; Esa, M.R.M.; Cooray, V.; Dutkiewicz, E. Interference from cloud-to-ground and cloud flashes in wireless communication system. *Electr. Power Syst. Res.* **2014**, *113*, 237–246. [\[CrossRef\]](#)
13. Hoole, P.R.P.; Sharip, M.R.M.; Fisher, J.; Pirapaharan, K.; Othman, A.K.H.; Julai, N.; Rufus, S.A.; Sahrani, S.; Hoole, S.R.H. Lightning Protection of Aircraft, Power Systems and Houses Containing IT Network Electronics. *J. Telecommun. Electron. Comput. Eng.* **2017**, *9*, 3–10.
14. Borisov, R.K.; Zhulikov, S.S.; Koshelev, M.A.; Maksimov, B.K.; Mirzabekyan, G.Z.; Turchaninova, Y.S.; Khrenov, S.I. A Computer-Aided Design System for Protecting Substations and Overhead Power Lines from Lightning. *Russ. Electr. Eng.* **2019**, *90*, 86–91. [\[CrossRef\]](#)
15. Lysov, N.; Temnikov, A.; Chernensky, L.; Orlov, A.; Belova, O.; Kivshar, T.; Kovalev, D.; Voevodin, V. Physical Simulation of the Spectrum of Possible Electromagnetic Effects of Upward Streamer Discharges on Model Elements of Transmission Line Monitoring Systems Using Artificial Thunderstorm Cell. *Appl. Sci.* **2021**, *11*, 8723. [\[CrossRef\]](#)
16. Temnikov, A.G. Using of artificial clouds of charged water aerosol for investigations of physics of lightning and lightning protection. In Processing of the 2012 International Conference on Lightning Protection (ICLP), Vienna, Austria, 2–7 September 2012. [\[CrossRef\]](#)
17. Makalsky, L.M.; Orlov, A.V.; Temnikov, A.G. Possible mechanism of lightning strokes to extra-high-voltage power transmission lines. *J. Electrostat.* **1996**, *37*, 249–260. [\[CrossRef\]](#)

18. Vasilyak, L.M.; Vereshchagin, I.P.; Glazkov, V.V.; Kononov, I.G.; Orlov, A.V.; Polyakov, D.N.; Sinkevich, O.A.; Sokolova, M.V.; Temnikov, A.G.; Firsov, K.N. Investigation of electric discharges in the vicinity of a charged aerosol cloud and their interaction with a laser-induced spark. *High Temp.* **2003**, *41*, 166–175. [\[CrossRef\]](#)
19. Temnikov, A.G.; Orlov, A.V.; Bolotov, V.N.; Tkach, Y.V. Studies of the parameters of a spark discharge between an artificial charged water-aerosol cloud and the ground. *Tech. Phys.* **2005**, *50*, 868–875. [\[CrossRef\]](#)
20. Temnikov, A.G.; Orlov, A.V.; Chernensky, L.L.; Bolotov, V.N.; Pisarev, V.P. Influence of model hydrometeors on the final stage of a discharge from an artificial charged water aerosol cloud. *Tech. Phys.* **2009**, *35*, 1437–1445. [\[CrossRef\]](#)
21. Temnikov, A.G.; Chernensky, L.L.; Orlov, A.V.; Lysov, N.Y.; Zhuravkova, D.S.; Belova, O.S.; Gerastenok, T.K. Application of Artificial Thunderstorm Cells for the Investigation of Lightning Initiation Problems between a Thundercloud and the Ground. *Therm. Eng.* **2017**, *64*, 994–1006. [\[CrossRef\]](#)
22. Temnikov, A.G. Investigation of peculiarities of discharge formation from the system of artificial charged aerosol clouds of negative polarity. *Electr. Power Syst. Res.* **2014**, *113*, 3–9. [\[CrossRef\]](#)
23. Temnikov, A.G.; Zhuravkova, D.S.; Orlov, A.V.; Lysov, N.Y. Outlook Research of Application of Model Hydrometeor Arrays for Artificial Initiation of Lightning and Thundercloud Charge Reduction. *IOP Conf. Ser. Mater. Sci. Eng.* **2019**, *698*, 044039. [\[CrossRef\]](#)
24. Temnikov, A.G.; Orlov, A.V. Determination of the electric field of a submerged turbulent jet of charged aerosol. *Electr. Technol.* **1996**, *3*, 49–62.
25. Vereshchagin, I.P.; Temnikov, A.G.; Orlov, A.V.; Stepanyanz, V.G. Computation of mean trajectories of charged aerosol particles in turbulent jets. *J. Electrostat.* **1997**, *40–41*, 503–508. [\[CrossRef\]](#)
26. Temnikov, A.G. Dynamics of electric field formation inside the artificially charged aerosol cloud and in a space near its boundaries. In Proceedings of the 12th International Conference on Atmospheric Electricity, Versal, France, 9–13 June 2003. ThC3-017-196.
27. Temnikov, A.G.; Chernensky, L.L.; Orlov, A.V.; Kivshar, T.K.; Lysov, N.Y.; Belova, O.S.; Zhuravkova, D.S. Peculiarities of the electric field calculation of the artificial thunderstorm cells. *Int. J. Circuits Syst. Signal Process.* **2018**, *12*, 305–311.
28. Rakov, V.A.; Uman, M.A. *Lightning: Physics and Effects*; Cambridge University Press: Boca Raton, FL, USA, 2003.
29. Syssoev, V.S.; Kostinskiy, A.Y.; Makalskiy, L.M.; Rakov, A.V.; Andreev, M.G.; Bulatov, M.U.; Sukharevsky, D.I.; Naumova, M.U. A Study of Parameters of the Counterpropagating Leader and its Influence on the Lightning Protection of Objects Using Large-Scale Laboratory Modeling. *Radiophys. Quantum Electron.* **2014**, *56*, 839–845. [\[CrossRef\]](#)
30. Kostinskiy, A.Y.; Syssoev, V.S.; Mareev, E.; Rakov, V.; Andreev, M.G.; Bogatov, N.; Makal'Sky, L.M.; Sukharevsky, D.I.; Aleshchenko, A.; Kuznetsov, V.; et al. Electric discharges produced by clouds of charged water droplets in the presence of moving conducting object. *J. Atmos. Sol. Terr. Phys.* **2015**, *135*, 36–41. [\[CrossRef\]](#)
31. Kostinskiy, A.Y.; Syssoev, V.S.; Bogatov, N.A.; Mareev, E.A.; Andreev, M.G.; Makalsky, L.M.; Sukharevsky, D.I.; Rakov, V.A. Infrared images of bidirectional leaders produced by the cloud of charged water droplets. *J. Geophys. Res. Atmos.* **2015**, *120*, 10,728–10,735. [\[CrossRef\]](#)
32. Kostinskiy, A.Y.; Syssoev, V.S.; Bogatov, N.A.; Mareev, E.A.; Andreev, M.G.; Makalsky, L.M.; Sukharevsky, D.I.; Rakov, V.A. Observation of a new class of electric discharges within artificial clouds of charged water droplets and its implication for lightning initiation within thunderclouds. *Geophys. Res. Lett.* **2015**, *42*, 8165–8171. [\[CrossRef\]](#)
33. Kostinskiy, A.Y.; Syssoev, V.S.; Bogatov, N.; Mareev, E.; Andreev, M.G.; Bulatov, M.U.; Makal'Sky, L.M.; Sukharevsky, D.I.; Rakov, V.A. Observations of the connection of positive and negative leaders in meter-scale electric discharges generated by clouds of negatively charged water droplets. *J. Geophys. Res. Atmos.* **2016**, *121*, 9756–9766. [\[CrossRef\]](#)
34. Rakov, V.A.; Mareev, E.A.; Tran, M.D.; Zhu, Y.; Bogatov, N.A.; Kostinskiy, A.Y.; Syssoev, V.S.; Lyu, W. High-Speed Optical Imaging of Lightning and Sparks: Some Recent Results. *IEEE Trans. Power Energy.* **2018**, *138*, 321–326. [\[CrossRef\]](#)
35. Mazur, V.A. *Principles of Lightning Physics*; IoP Publishing: Bristol, UK; New York, NY, USA, 2016.
36. Sharma, S.R.; Cooray, V.; Fernando, M.; Miranda, F.J. Temporal features of different lightning events revealed from wavelet transform. *J. Atmos. Sol. Terr. Phys.* **2011**, *73*, 507–515. [\[CrossRef\]](#)
37. Esa, M.R.M.; Ahmad, M.R.; Cooray, V. Wavelet analysis of the first electric field pulse of lightning flashes in Sweden. *Atmos. Res.* **2014**, *138*, 253–267. [\[CrossRef\]](#)
38. Temnikov, A.G.; Chernensky, L.L.; Belova, O.S.; Orlov, A.V.; Zimin, A.S. Spectral characteristics of discharges from artificial charged aerosol cloud. In Proceedings of the IEEE Conference Publications: Lightning Protection (ICLP), Proceedings of the 2012 International Conference on Lightning Protection, Shanghai, China, 11–18 October 2014. Article number 6973333.
39. Cooray, V. *Lightning Electromagnetics*; IET Publishing: London, UK, 2012.
40. Cooray, V.; Cooray, G. Electromagnetic fields of accelerating charges: Applications in lightning protection. *Electr. Power Syst. Res.* **2017**, *145*, 234–247. [\[CrossRef\]](#)
41. Cooray, V.; Cooray, G. The Electromagnetic Fields of an Accelerating Charge: Applications in Lightning Return-Stroke Models. *IEEE Trans. Electromagn. Compat.* **2010**, *52*, 944–955. [\[CrossRef\]](#)
42. Cooray, V.; Cooray, G. Electromagnetic radiation field of an electron avalanche. *Atmos. Res.* **2012**, *117*, 18–27. [\[CrossRef\]](#)
43. Shi, F.; Liu, N.; Dwyer, J.R.; Ihaddadene, K.M.A. VHF and UHF Electromagnetic Radiation Produced by Streamers in Lightning. *Geophys. Res. Lett.* **2019**, *46*, 443–451. [\[CrossRef\]](#)

- 
44. Gushchin, M.E.; Korobkov, S.V.; Zudin, I.Y.; Nikolenko, A.S.; Mikryukov, P.A.; Syssoev, V.S.; Sukharevsky, D.I.; Orlov, A.I.; Naumova, M.Y.; Kuznetsov, Y.A.; et al. Nanosecond electromagnetic pulses generated by electric discharges: Observation with clouds of charged water droplets and implications for lightning. *Geophys. Res. Lett.* **2021**, *48*, e2020GL092108. [[CrossRef](#)]
  45. Rochelle, P. ORBCOMM Announces Commercial Service for Its Final 11 OG2 Satellites. 1 March 2016. Available online: <https://www.orbcomm.com/en/company-investors/news/2016/orbcomm-announcescommercial-service-for-its-final-11-og2-satellites> (accessed on 30 August 2021).
  46. Our Mission Is Space Communication. Available online: <http://www.gonets.ru/eng/company/mission/> (accessed on 30 August 2021).